

PION CLOUD CONTRIBUTION TO K^+ NUCLEUS SCATTERING

C. García-Recio⁽¹⁾, J. Nieves⁽²⁾ and E. Oset⁽³⁾

⁽¹⁾ Dpto. de Física Moderna, Facultad de Ciencias, Universidad de Granada,
E-18071 Granada, Spain.

⁽²⁾ Physics Department, The University, Southampton SO9 5NH, United Kingdom.

⁽³⁾ Dpto. de Física Teórica and IFIC, Centro Mixto Universidad de Valencia-CSIC.
E-46100 Burjassot, (Valencia), Spain.

Abstract

A careful reanalysis is done of the contribution to K^+ nucleus scattering from the interaction of the kaon with the virtual pion cloud. The usual approximations made in the evaluation of the related kaon selfenergy are shown to fail badly. We also find new interaction mechanisms which provide appreciable corrections to the kaon selfenergy. Some of these contribute to the imaginary part below pion creation threshold. The inclusion of these new mechanisms in the inelastic part of the optical potential produces a significant improvement in the differential and total K^+ nuclear cross sections. Uncertainties remain in the dispersive part of the optical potential.

PACS numbers: 25.80.Nv, 24.10.C, 13.75-n, 21.65.+f

Submitted to Physical Review C

Preprint number: UG-DFM-2/94

1.- Introduction

Systematic discrepancies between the microscopic optical potential calculations for K^+ nucleus scattering [1, 2, 3] and the experimental data [4, 5, 6, 7, 8] have led to suggestions that it may be an indication of an increased size of the nucleons in the nucleus [2, 9, 10]. These discrepancies remain when a number of conventional nuclear corrections (Pauli blocking, nucleon-nucleon correlations, off-shell corrections, etc) are taken into account ([2]-[3]). Parallelly, work has been done about the contribution of the nuclear pion cloud to the K^+ optical potential [11, 12]. In [11] a qualitative estimate is done of the meson cloud effects by assuming that the K^+N cross section is increased by $\delta n_\pi \sigma(K^+\pi)$, where δn_π is the excess number of pions per nucleon in the nucleus. In ref. [12], together with a good summary of the status of the problem, a thorough and instructive study of the meson cloud contribution to the scattering amplitude is done by evaluating explicitly the real and the imaginary parts. A $K^+\pi$ amplitude with off-shell extrapolation and crossing symmetry, inspired in the work on the $\pi\pi$ interaction [13] is used. The work relies upon the pion excess distribution found in [14], which accounts for ph and Δh components in a correlated ground state. The interference of ph and Δh components is essential to produce a positive pion excess number in the nucleus [14, 15].

In the present work we have made a more rigorous evaluation of the pion cloud contribution to the K^+ nucleus optical potential which requires only the knowledge of the pion propagator in the nuclear medium and a realistic model for the $K\pi$ amplitude.

In the nuclear medium, the pion propagator is renormalized by allowing the pion excite ph and Δh components, such a model provides a realistic model for the π nucleus interaction and accounts for the basic components needed to produce realistic pion numbers in finite nuclei [15]. Our model for the pion propagator is briefly described in Appendix A. The pion distribution is not needed explicitly in our computation of the K^+ -nucleus optical potential, although the formal connection of the pion propagator to the pion distribution, $n(\mathbf{q})$, will be made. Actually, one of our findings is that the pion cloud contribution to the imaginary part of the K^+ - nucleus optical potential can not be cast as an integral of the form $\int d^3\mathbf{q} n(\mathbf{q}) f(\mathbf{q})$ as assumed in [12] and also implicitly in [11].

For the $K\pi$ amplitude we use the model of ref. [12]. This model incorporates on-shell conditions and crossing symmetry. A detailed study is made in ref. [12] about uncertainties from the off-shell extrapolation, form factors, etc., allowing us to simplify the discussions and concentrate on the novelties that the present work introduces. For the sake of completeness, in Appendix B this $K\pi$ model is summarized.

On the other hand, we introduce new mechanisms also related to the scattering of positive kaons with the pion cloud, which have not been considered previously and are found to be very important.

The calculations are done in infinite nuclear matter and the contributions to the K^+ selfenergy are obtained as a function of ρ , the nuclear matter density. By means of the local density approximation, carefully studied and justified in [16]

in connection with π -nucleus scattering, we obtain the meson exchange currents (MEC) contribution to the K -nucleus optical potential as a function of $\rho(r)$. Our model for the K -nucleus potential is obtained by adding these new contributions, calculated in the present work, to the conventional ones from the impulse approximation (see Appendix C) and to the standard nuclear corrections (nuclear correlations, off-shell and binding effect, Pauli exclusion,... calculated in refs. [2, 6]). This new optical potential is then used to obtain the differential and total K^+ -nucleus cross sections by solving numerically the Klein Gordon equation. In the following, we will refer indistinctly to the kaon selfenergy or to the optical potential, as they are related by $\Pi(k) = 2k^0 V_{\text{opt}}(k)$. Nevertheless it is the selfenergy what appears in the Klein-Gordon equation.

The paper is organized as follows: In order to test the model used for pions in nuclei, the excess number of pions in the nucleus is calculated in section 2. In section 3 we recalculate the contribution from the MEC mechanism considered in refs. [11, 12] but relaxing the static approximation. The new MEC mechanisms contributing to the the K^+ selfenergy in nuclei are presented in section 4 where is also evaluated their contribution to the imaginary part of the K^+ -nucleus optical potential. Section 5 is devoted to the study of the MEC contribution to the real part of K^+ selfenergy. In section 6, the K^+ -nucleus differential and total cross-sections calculated with IA, with IA+MEC, and with the conventional optical potential plus MEC, are shown and compared with experimental data for ^{12}C and ^{40}Ca and also with the ratio of those cross-sections over the K^+ deuterium cross-section. Finally, in section 7, we summarize and parametrize the results for the MEC contribution to the K^+ optical potential and present our conclusions.

2.- The pion propagator and the number of pions.

The propagator of a pion with four-momentum q (and isospin λ) should satisfy the Lehmann representation [17]

$$D(q) = \int_0^\infty \frac{d\omega}{\pi} (-2\omega) \frac{\text{Im}D(\omega, \mathbf{q})}{q^0 - \omega^2 + i\epsilon} , \quad (1)$$

Our calculation of the pion propagator in Appendix A preserves the appropriate analytical properties and therefore eq. (1) holds.

Another equation which is relevant in connection with the present problem is the sum rule

$$-\int_0^\infty \frac{dq^0}{\pi} 2q^0 \text{Im}D(q^0, \mathbf{q}) = 1. \quad (2)$$

This equation expresses the equal time commutation relation of the pion fields. We check that eq. (2) is fulfilled in our model at the level of one per thousand which is sufficient for our purposes.

A check of the model for pion propagation in the nucleus is to calculate the number of pions it produces. Although this quantity is not needed in our evaluation

of the pion cloud contribution to the K^+ nucleus scattering, we show our results for it in order to compare with earlier work. Let $n_\lambda(\mathbf{q})$ be the pion number distribution for a single class of pions and $n(\mathbf{q})$ the total number of pions, namely

$$n(\mathbf{q}) \equiv \sum_\lambda n_\lambda(\mathbf{q}) = \sum_\lambda \langle a_{\mathbf{q}\lambda}^+ a_{\mathbf{q}\lambda} \rangle, \quad (3)$$

where the symbol $\langle \rangle$ indicates the expectation value in the nuclear ground state and $a_{\mathbf{q}\lambda}$ the annihilation operator of a pion with momentum \mathbf{q} and isospin λ . Thus,

$$\int \frac{d^3\mathbf{q}}{(2\pi)^3} n(\mathbf{q}) = \frac{n_\pi}{V} = \frac{n_\pi}{A} \rho, \quad (4)$$

with n_π/A the total number of pions per nucleon. More amenable to calculation are the quantities $N(\mathbf{q})$ and $\delta N(\mathbf{q})$,

$$N(\mathbf{q}) = n(\mathbf{q}) + \frac{1}{2} \sum_\lambda \langle a_{\mathbf{q},\lambda}^+ a_{-\mathbf{q},-\lambda}^+ \rangle + \frac{1}{2} \sum_\lambda \langle a_{\mathbf{q},\lambda} a_{-\mathbf{q},-\lambda} \rangle, \quad (5)$$

$$\delta N(\mathbf{q}) = N(\mathbf{q}) - \rho \left(\frac{\partial N(\mathbf{q})}{\partial \rho} \right)_{\rho=0} \quad (6)$$

The linear term in ρ accounts for the number of pions per free nucleon, then it is subtracted in eq. (6) to obtain the “pion excess” $\delta N(\mathbf{q})$.

According to eq. (4) the following integral

$$\frac{1}{\rho} \int \frac{d^3\mathbf{q}}{(2\pi)^3} \delta N(\mathbf{q}) \equiv \frac{\delta N_\pi}{A}. \quad (7)$$

provides the “excess number of pions” per nucleon, counting the three isospin states and also $\langle a_{\mathbf{q},\lambda}^+ a_{-\mathbf{q},-\lambda}^+ \rangle$ and $\langle a_{\mathbf{q},\lambda} a_{-\mathbf{q},-\lambda} \rangle$ as it comes from eq. (5). According to the results of ref [18] on the contribution of the pion cloud to Compton scattering, $n_\lambda(\mathbf{q})$ is equal to $\frac{1}{2} \langle a_{\mathbf{q},\lambda}^+ a_{-\mathbf{q},-\lambda}^+ \rangle + \frac{1}{2} \langle a_{\mathbf{q},\lambda} a_{-\mathbf{q},-\lambda} \rangle$, then the results of previous papers on the pion number excess $\delta n(\mathbf{q})$ and δn_π are to be compared with $\delta N(\mathbf{q})/2$ and $\delta N_\pi/2$.

These quantities can be computed using the relationships

$$\frac{1}{3} N(\mathbf{q}) = -2\omega(\mathbf{q}) \int_0^\infty \frac{dq^0}{2\pi} \text{Im}[D(q) - D_0(q)] \quad (8)$$

$$\frac{1}{3} \delta N(\mathbf{q}) = -2\omega(\mathbf{q}) \int_0^\infty \frac{dq^0}{2\pi} \text{Im}[\delta D(q)] \quad (9)$$

where $\omega(\mathbf{q}) = \sqrt{m_\pi^2 + \mathbf{q}^2}$ and

$$\delta D(q) = D(q) - D_0(q) - \rho \left(\frac{\partial D(q)}{\partial \rho} \right)_{\rho=0}. \quad (10)$$

Eq. (8) can be derived by writing the pion propagator in terms of the creation and annihilation operators and making use of eq. (1)

In fig. 1, we show $\delta N(\mathbf{q})$ (solid line) for normal ($\rho = \rho_0 = 0.17 \text{ fm}^{-3}$) nuclear matter. We have also calculated $\delta N(\mathbf{q})$ for different values of the density, observing that it behaves quadratically in density. If only ph excitations are considered one obtains the dotted line in fig. 1. By integrating it a negative pion excess number is obtained as it was already pointed out in [12]. If only Δh excitations are considered one obtains the result of the dashed line, which represents a very small pion excess number. When considering simultaneously both, ph and Δh , excitations the solid line of fig. 1 is obtained. $\delta N(\mathbf{q})$ is larger for large \mathbf{q} than before and a positive excess number of pions is found when integrating over $d^3\mathbf{q}$, thus proving that the interference of ph and Δh is essential to produce a positive excess number.

The distribution $\delta N(\mathbf{q})$ has identical shape to the one from [14]. For $\rho = \rho_0$ the integral of eq. (7) gives 0.67, half of it coming from the integral of the strict pion number, $\delta n(\mathbf{q})$, according to [18]. This gives us 0.33 pions per nucleon in nuclear matter at $\rho = \rho_0$. Since $\int d^3\mathbf{q} \delta N(\mathbf{q})$ is proportional to ρ^2 and in a finite nucleus like ^{12}C the magnitude $\frac{1}{A} \int d^3\mathbf{r} \rho^2(\mathbf{r})$ is around a factor two smaller than in nuclear matter, then we obtain 0.17 pions per nucleon in the ^{12}C nucleus, on the upper edge of the band of values obtained by other authors [14, 15].

3.- Formal derivation of the “standard” pion cloud contribution

We call here “standard” mechanism, to the one depicted in fig. 2. This is the only one considered in previous papers, and then it was calculated in the static approach which we describe in subsection 3.1. In subsection 3.2 we calculate it exactly.

The K^+ selfenergy of the basic diagram shown in fig.2a in an infinite spin-isospin symmetric nuclear medium is given by

$$-i\Pi(k) = \int \frac{d^4q}{(2\pi)^4} iD(q) (-i) \frac{1}{2} 3 t^0(k, q; k, q), \quad (11)$$

where t^0 is the isoscalar $K^+\pi$ amplitude (average of $t_{K^+\pi^i}$ for the three charged pions) and the factor $\frac{1}{2}$ is a symmetry factor. However, as depicted in figs. 2b, 2c, 2d the full propagator contains the free pion, one ph or Δh corrections and higher order corrections with $2ph$, $ph \Delta h$, $2\Delta h$, etc, excitations. The contribution from the free pion has to be subtracted because it corresponds to a piece in the free K^+ selfenergy. Analogously, once this subtraction is made, we will have terms in the selfenergy coming from $1ph$ or $1\Delta h$ excitations which are proportional to ρ . These terms must also be subtracted because they are implicitly accounted for in the IA selfenergy $\Pi^{\text{IA}} = t_{KN} \rho$, where t_{KN} is the empirical KN t -matrix. Hence the genuine pion cloud contribution to the K^+ selfenergy is given by

$$\delta\Pi(k) = i \int \frac{d^4q}{(2\pi)^4} \delta D(q) \frac{3}{2} t^0(k, q; k, q), \quad (12)$$

3.1.- Static Approximation

In the static approximation the q^0 dependence in the t matrix is neglected. For instance in [12] q^0 is set to zero in $t^0(k, q; k, q)$. In this case one obtains

$$\begin{aligned}\delta\Pi_{\text{stat}}(k) &= -\int \frac{d^3\mathbf{q}}{(2\pi)^3} \int_0^\infty \frac{dq^0}{2\pi} \text{Im}\delta D(q) 3 \left[t^0(k, q; k, q) \right]_{q^0 \text{fix}} \\ &= \int \frac{d^3\mathbf{q}}{(2\pi)^3} \frac{\delta N(\mathbf{q})}{2\omega(\mathbf{q})} t^0(k, q; k, q) \Big|_{q^0 \text{fix}},\end{aligned}\quad (13)$$

where the first equality follows from $\int dq^0 \text{Re}D(q) = 0$, and $D(q^0, \mathbf{q}) = D(-q^0, \mathbf{q})$.

Hence, in the static approximation $\Pi(k)$ comes as a weighted integral of the $K^+\pi$ amplitude with the pion distribution in the nucleus. This result looks intuitive but recall that $N(\mathbf{q})$ contains $n(\mathbf{q})$ and also the expectation values $\langle a_{\mathbf{q}\lambda} a_{-\mathbf{q}-\lambda} \rangle$ and $\langle a_{\mathbf{q}\lambda}^+ a_{-\mathbf{q}-\lambda}^+ \rangle$. These three factors correspond in fact to having the K^+ scattering with a pion, annihilating two pions from the ground state or creating two pions from the ground state, as symbolically depicted in fig. 3. Note that with our field theoretical formalism, the three terms are automatically included.

The approach of [12] corresponds to the static approximation of eq. (13) with $\delta N(\mathbf{q}) = 2 \times \delta n(\mathbf{q})$ and $\delta n(\mathbf{q})$ taken from [14]. The factor 2 accounts for the two pion creation or annihilation mechanisms as found in [18]. As already noted in [12] these extra terms are ignored in the approach of [11].

Our claim here is that the static approximation which justifies the approaches of [11, 12] is inaccurate, particularly for the imaginary part of $\Pi(k)$.

Indeed, the imaginary part of $\delta\Pi_{\text{stat}}$ from eq. (13) is given by

$$\text{Im}\delta\Pi_{\text{stat}}(k) = -\int \frac{d^3\mathbf{q}}{(2\pi)^3} \int_0^\infty \frac{dq^0}{2\pi} \text{Im}\delta D(q) 3 \left[\text{Im}t^0(k, q; k, q) \right]_{q^0 \text{fix}}. \quad (14)$$

Note that the range of the q^0 integration goes from 0 to ∞ . This will be very different in the exact case which we analyze below, implying, as we shall see, that the static approximation is not good.

3.2.- Exact Calculation of $\text{Im}\delta\Pi$ for the “standard” mechanism

Now let us find the exact expression for $\text{Im}\delta\Pi(k)$. This requires a knowledge of the analytical structure of $t^0(k, q; k, q)$. We assume that this amplitude can be written in the following way:

$$t^0(k, q; k, q) = \tilde{t}(s) + \tilde{t}(u), \quad (15)$$

where $s = (k + q)^2$, $u = (k - q)^2$ are the usual Mandelstam variables ($t = 0$ in our case), which automatically satisfies crossing symmetry. This is the case for the model which we will use. The function $\tilde{t}(x)$ has the right analytical properties and develops an imaginary part for $x > x_0 = (m_K + m_\pi)^2$. It also satisfies the subtracted dispersion relation [17, 19]

$$\tilde{t}(s) = P(s) + (s - x_0) \int_{x_0}^\infty \frac{dx}{\pi} \frac{\text{Im} \tilde{t}(x)}{(s - x + i\epsilon)(x_0 - x)}, \quad (16)$$

where $P(x)$ is a real polynomial.

Using this form of t^0 from eq. (15) in $\delta\Pi$ of eq. (12) and the symmetry of the integrand under $q \leftrightarrow -q$. we obtain:

$$\delta\Pi(k) = i3 \int \frac{d^4q}{(2\pi)^4} \delta D(q) \tilde{t}(u) \quad (17)$$

The analytical structure of $\delta D(q)\tilde{t}(u)$ in the variable q^0 is shown in fig. 4. It has cuts and poles in the second and fourth quadrants from $\delta D(q)$ and two single poles in $q^0 = k^0 \pm E(x) \mp i\epsilon$, with $E(x) = [(k - q)^2 + x]^{1/2}$. This particular structure suggests a Wick rotation, as indicated in fig. 4, in order to perform the q^0 integral. Since the integral vanishes at the circles of infinite radius, we have

$$i \int_{-\infty}^{\infty} dq^0 = i \int_{-i\infty}^{i\infty} dq^0 - 2\pi \operatorname{Res}(q^0 = k^0 - E(x)) \theta(k^0 - E(x)), \quad (18)$$

The integral over the imaginary axis is real and the only source of imaginary part comes from the residue at the pole. Thus,

$$\begin{aligned} \operatorname{Im} \delta\Pi(k) &= \\ &= - \int \frac{d^3\mathbf{q}}{(2\pi)^3} \int_{x_0}^{\infty} \frac{dx}{\pi} \theta(k^0 - E(x)) \frac{\operatorname{Im}\tilde{t}(x)}{2E(x)} 3\operatorname{Im} \delta D(q)|_{q^0=k^0-E(x)} \\ &= - \int \frac{d^3\mathbf{q}}{(2\pi)^3} \theta(k^0 - E(x_0)) \int_0^{k^0 - E(x_0)} \frac{dq^0}{2\pi} 6\operatorname{Im}\tilde{t}(u) \operatorname{Im} \delta D(q). \end{aligned} \quad (19)$$

Note that \tilde{t} appears at the end with argument u rather than s . By comparing eq. (19) with the static expression of eq. (14) we find a main substantial difference in the fact that the q^0 integral goes from 0 to ∞ in the static formula while here it is restricted to the interval $[0, k^0 - E(x_0)]$. Hence, even if we make $\operatorname{Im}\tilde{t}(u)$ static in eq. (19) in order to take it out of the q^0 integral, the pion excess number $\delta N(\mathbf{q})$ will not be generated because the range $[0, \infty]$ in the q^0 integration is needed in eq. (9). Note that the range of \mathbf{q} is also restricted because $E(x_0) < k^0$. Then the whole phase space allowed is finite, as corresponds to the reaction channels accounted for by $\operatorname{Im}\Pi(k)$. Under these circumstances one should not expect the static approximation to provide realistic results.

The pathologies generated by the intuitive use of the particle number are general in decay processes or in the evaluation of imaginary parts of amplitudes, i.e., in cases where conservation of energy and momentum is at stake. This occurs because the relevant magnitude is $\operatorname{Im}D(q)$ which provides the probability of finding a pion with momentum \mathbf{q} and energy q^0 . The probability of finding a pion of momentum \mathbf{q} is an integral property obtained when one integrates over the energy of the pion from 0 to ∞ . However, in decay processes the range of energies allowed is limited because of energy and momentum conservation, and the particle number can not be factored out. A spectacular example of the failure of the static approximation has been shown in [20] in connection with the mesonic Λ decay in nuclei. The argument goes as follows: The $\Lambda \rightarrow \pi N$ decay is forbidden

in nuclei because the nucleon momentum, $k_N \simeq 100\text{MeV}/c$ is below the Fermi momentum $k_F \simeq 270\text{MeV}/c$ (because of surface effects the decay is still possible but appreciable reduced, about 4 orders of magnitude in heavy nuclei). However, since the occupation number for states below the Fermi momentum is not 1 but about 0.85, it was implicitly argued in [21] that the Λ mesonic decay in nuclei should saturate at values about 15% of the free Λ width [up to a moderate effect of pion absorption in the nucleus]. The argument, however intuitive, suffers from the same defects of the static approximation discussed here and it was found in [20] that, the actual results for the mesonic width are about three orders of magnitude smaller than the results of the intuitive argument based on the nucleon distribution in nuclei.

The interesting expression for $\text{Im}\delta\Pi(k)$ of eq. (19) indicates that one needs only $\text{Im}D(q)$ and $\text{Im}\tilde{t}(u)$ to obtain $\text{Im}\delta\Pi(k)$ and only in a reduced range of q^0 and q . Although one can in principle evaluate $\text{Im}\delta\Pi(k)$ from eq. (12), it is a highly inefficient and dangerous method because of the strong cancellations and the large ranges of q^0 involved in the integrations.

For the real part of $\delta\Pi$ we do not find finite ranges of integration.

3.3.- Results of calculations for $\text{Im}\delta\Pi$

For the explicit calculations we use the $K^+\pi$ amplitude from ref. [12], which is summarized in Appendix B. Calculations with different values of ρ have shown that $\text{Im}\delta\Pi$ behaves quadratically in density. In fig. 5 we present the imaginary part of the K^+ selfenergy calculated for nuclear matter at normal density ρ_0 . The dot-dashed line is the result of the static approximation using q^0 fixed to zero. The dashed line displays the exact result calculated as explained in subsection 3.2. The leading part of the optical potential comes from the IA. For comparison, it is displayed in the figure with a crossed solid line. We observe that the static result is about twice the exact one, and also that in any case both of them are very small compared to the IA. Then this mechanism is not enough to account for the experimental results. For comparison we also show there the results of the total MEC contribution when considering the new mechanisms which we discuss below.

4.- New mechanisms from the pion cloud.

The imaginary part of $\delta\Pi$ of fig. 2 is related to $\text{Im}\delta D$ and $\text{Im}t_{K\pi}$ by eq. (19). This means that the reactive channels of the K^+ selfenergy are due simultaneously to the reaction channels of the pion in nuclear matter and the reaction channels of $t_{K\pi}$. For the kaon kinetic energies which will be considered in this work the only open channels in $t_{K\pi}$ are the elastic one or the charge exchange, $K^+\pi_i \rightarrow K^0\pi_j$, and thus $\text{Im}t_{K\pi}$ is due only to the process $K\pi \rightarrow K\pi$. Hence, $\text{Im}t_{K\pi}$ is related through the optical theorem to $|t_{K\pi}|^2 \text{Im}D_0 \text{Im}D_K$ as it is given diagrammatically in fig. 6. Then, using the optical theorem in eq. (19), we obtain the identity shown diagrammatically in fig. 7. This allows us to understand the processes to which $\text{Im}\delta\Pi$ is due, these are: $K N \rightarrow K \pi N$, $K N \rightarrow K \pi \Delta$, where the interaction

KN is renormalized in the medium. The incoming K^+ has to produce a kaon, a free pion and a nuclear excitation, so it is clear why the kinetic energy of the K^+ must be larger than the pion mass as shown in fig. 5.

Looking again at fig. 7 one realizes that not only one pion, but also the other pion and also both pions simultaneously must be modified by the nuclear medium. (The same applies to the intermediate kaon, but we will see that the kaon modification in the medium is negligible as compared to pion modification).

The imaginary part of the kaon selfenergy due to the pion cloud is given by the diagram of fig. 8, except that its linear part in density is to be subtracted to eliminate selfenergy parts which are already included in the IA. Let $\tilde{\Pi}(k)$ be the K^+ selfenergy of the diagram of fig. 8, then the pionic cloud or MEC contribution to the K^+ selfenergy, Π^{MEC} , is given by:

$$\text{Im}\Pi^{\text{MEC}}(k) = \text{Im}\tilde{\Pi}(k) - \rho \left(\frac{\partial \text{Im}\tilde{\Pi}(k)}{\partial \rho} \right)_{\rho=0} - (\text{Im}\tilde{\Pi}(k))_{\rho=0}, \quad (20)$$

but $(\text{Im}\tilde{\Pi}(k))_{\rho=0} = 0$ if the kaon is on-shell because a free kaon is stable under strong interactions.

The K^+ selfenergy associated to the diagram of fig. 8 is given by:

$$\begin{aligned} \tilde{\Pi}(k) &= -\frac{1}{2} \int \frac{d^4 q}{(2\pi)^4} \int \frac{d^4 q'}{(2\pi)^4} D(q') D(q) D_K(k') \\ &\times \sum_{ijl} t_{K^+\pi^i \rightarrow K^l\pi^j}(k', q'; k, -q) t_{K^l\pi^j \rightarrow K^+\pi^i}(k, -q; k', q') \Big|_{k'=k-q-q'} \end{aligned} \quad (21)$$

Its imaginary part is easily evaluated by means of Cutkosky rules [17]: in all intermediate states cut by the dotted line substitute:

$$\begin{aligned} \Pi(k) &\rightarrow 2i\theta(k^0)\text{Im}\Pi(k) \\ D(q) &\rightarrow 2i\theta(q^0)\text{Im}D(q) \\ D_K(q) &\rightarrow 2i\theta(q^0)\text{Im}D_K(q) \end{aligned} \quad (22)$$

and put complex conjugate the amplitude above the dotted line. Thus, by taking the imaginary part corresponding to cutting the three meson propagators as shown by the horizontal line of fig. 8, one obtains:

$$\begin{aligned} \text{Im}\tilde{\Pi}(k) &= 2 \int \frac{d^4 q}{(2\pi)^4} \int \frac{d^4 q'}{(2\pi)^4} \theta(q^{0'})\theta(q^0)\theta(k^{0'})\text{Im}D(q')\text{Im}D(q)\text{Im}D_K(k') \\ &\times \sum_{\alpha} |t_{K\pi}^{\alpha}(k', q'; k, -q)|^2 \Big|_{k'=k-q-q'} \end{aligned} \quad (23)$$

where α runs over the indices i, j, l in $K^+\pi^i \rightarrow K^l\pi^j$.

By expanding the pion propagators above in powers of the density, $D = D_0 + D_{(1)} + \delta D$ (being $D_{(1)}$ of order ρ , and δD the remaining terms of higher orders),

and using the symmetry $q \leftrightarrow q'$ (which holds due to the crossing symmetry of the amplitudes), we obtain:

$$\begin{aligned} \text{Im}\tilde{\Pi}(k) &= 2 \int \frac{d^4 q}{(2\pi)^4} \int \frac{d^4 q'}{(2\pi)^4} \theta(q^0) \theta(q^{0'}) \theta(k^{0'}) \text{Im}D_K(k') \\ &\times \sum_{\alpha} |t_{K\pi}^{\alpha}(k', q'; k, -q)|^2 \Big|_{k'=k-q-q'} \{ \text{Im}D_0(q') \text{Im}[D_0(q) + 2D_{(1)}(q) + 2\delta D(q)] \\ &\quad + \text{Im}D_{(1)}(q') \text{Im}D_{(1)}(q) + \mathcal{O}(\rho^3) \}. \end{aligned} \quad (24)$$

where the terms in $\delta D D_{(1)}$ and $\delta D \delta D$, of at least order ρ^3 , have been neglected. The term with $\text{Im}D_0(q') \text{Im}D_0(q)$ and the term with $2\text{Im}D_0(q') \text{Im}D_{(1)}(q)$ have to be subtracted because they are of zeroth and first order in density, respectively; and the terms with $2\text{Im}D_0(q') \text{Im}\delta D(q)$ and $\text{Im}D_{(1)}(q') \text{Im}D_{(1)}(q)$ must be kept since they are quadratic in density.

By subtracting the terms constant and linear in ρ we obtain the contributions to $\text{Im}\Pi^{\text{MEC}}$. Those contributions are diagrams $d1$, $d2$, $d3$ and $d4$ depicted in fig. 9, and their explicit expressions are given by:

$$\begin{aligned} \text{Im}\Pi^{\text{MEC}}(k) &= 2 \int \frac{d^4 q}{(2\pi)^4} \int \frac{d^4 q'}{(2\pi)^4} \theta(q^{0'}) \theta(q^0) \theta(k^{0'}) \text{Im}D_K(k') \\ &\times \sum_{\alpha} |t_{K\pi}^{\alpha}(k', q'; k, -q)|^2 \Big|_{k'=k-q-q'} \{ 2\text{Im}D_0(q') \text{Im}\delta D(q) \quad (d1) \\ &\quad + \text{Im}D_{(1)}(q') \text{Im}D_{(1)}(q) \} \quad (d2 + d3 + d4) . \end{aligned} \quad (25)$$

Now we consider the first term, diagram $d1$. If we look at the diagram of fig. 6b we can write the amplitude for this process following the same rules used so far and by means of Cutkosky rules, we obtain:

$$\begin{aligned} 3\text{Im}\tilde{t}(s') &= \quad (26) \\ -2 \int \frac{d^4 q'}{(2\pi)^4} \sum_{\alpha} &|t_{K\pi}^{\alpha}(k', q'; k, p)|^2 \theta(q^{0'}) \theta(k^{0'}) \text{Im}D_0(q') \text{Im}D_K(k') \Big|_{k'=k+p-q'}, \end{aligned}$$

with $s' = (k + p)^2$. If we substitute this in eq. (25) we find

$$\text{Im}\Pi^{d1}(k) = -6 \int \frac{d^3 q}{(2\pi)^3} \int_0^{\infty} \frac{dq^0}{2\pi} \text{Im}\tilde{t}(u) \text{Im}\delta D(q) = \text{Im}\delta\Pi(k) , \quad (27)$$

which is the same result as eq. (19). At the first sight the upper limit in the q^0 integration in eq. (26) is different than in eq. (19), but the condition $\text{Im}\tilde{t}(u) \neq 0$ makes q^0 smaller than $k^0 - E(x_0)$, and we regain the same limit. It is interesting to note that in spite of renormalizing the only existing pion line in eq. (19) one obtains the same result as here where we have renormalized either of the two pions in fig. 7b. The reason is that the use of a crossing symmetric amplitude and the equal contribution of the terms $\text{Im}\tilde{t}(s)$ and $\text{Im}\tilde{t}(u)$ of eq. (15) in eq. (19) accounts

for that. This can be better visualized if we make use of a model $K^+\pi^-$ scattering consisting of a resonant K^* pole (as in the p -wave amplitude of the model we use). If in fig. 6b and fig. 6c we renormalize and fold the external pion we obtain two diagrams like in fig. 7b where in one case one pion is renormalized and in the other case the other pion is renormalized. Hence we conclude that $\text{Im}\Pi^{d1}(k)$ is exactly the same contribution obtained before in eq. (19). However, we get now new contributions from the terms $d2$, $d3$, $d4$ which renormalize the two pions simultaneously.

The second term in $\text{Im}\Pi^{\text{MEC}}$ comes from $\text{Im}D_{(1)}\text{Im}D_{(1)}$. It contains new reaction channels, namely, the K^+ decaying into $K ph ph$, $K ph \Delta h$ and $K \Delta h \Delta h$. These have not been considered before. To evaluate them we need $\sum_{\alpha} |t_{K\pi}^{\alpha}(k, -q; k', q')|^2$ with the t -matrix off-shell for both q and q' . Given the small contribution from the p -wave part, the only one with an angular dependence in q' , we substitute $|t_{K\pi}|^2$ by an angular average in eq. (26), and hence we find for $u > (m_{\pi} + m_K)^2$

$$\sum_{\alpha} |t_{K\pi}^{\alpha}(k', q'; k, -q)|_{\text{ave}}^2 = \frac{-3\text{Im}\tilde{t}(u)}{2 \int \frac{d^4 q'}{(2\pi)^4} \theta(k^{0'}) \text{Im}D_K(k') \theta(q^{0'}) \text{Im}D_0(q') \Big|_{k' = k - q - q'}} \quad (28)$$

which after the evaluation of the denominator gives

$$\sum_{\alpha} |t_{K\pi}^{\alpha}(k', q'; k, -q)|_{\text{ave}}^2 = -\frac{8\pi\sqrt{u}}{q_{\text{CM}}} 3\text{Im}\tilde{t}(u) \simeq f(u). \quad (29)$$

with $u = (k - q)^2$ and q_{CM} the $K^+\pi$ CM momentum for K^+ and π on-shell. The function $f(u)$ for any value of u , in the model which we use, is explicitly written in appendix B, where some approximations are made which are consistent with the model itself. Now we use $f(u)$ to calculate the new channels. By expanding the first medium correction to the pion propagator into ph and Δh components as $D_{(1)} = D_{(1)}^{ph} + D_{(1)}^{\Delta h}$, one obtains:

$$\text{Im}\Pi^{\text{MEC}}(k) = \text{Im}\delta\Pi(k) + \quad (d1)$$

$$+ 2 \int \frac{d^4 q}{(2\pi)^4} \int \frac{d^4 q'}{(2\pi)^4} \theta(q^0) \theta(q^{0'}) \theta(k^{0'}) \text{Im}D_K(k') f((k - q)^2) \quad (30)$$

$$\times \{ \text{Im}D_{(1)}^{ph}(q') \text{Im}D_{(1)}^{ph}(q) + \quad (d2)$$

$$+ \text{Im}D_{(1)}^{ph}(q') \text{Im}D_{(1)}^{\Delta h}(q) + \text{Im}D_{(1)}^{ph}(q) \text{Im}D_{(1)}^{\Delta h}(q') + \quad (d3)$$

$$+ \text{Im}D_{(1)}^{\Delta h}(q') \text{Im}D_{(1)}^{\Delta h}(q) \} \quad (d4)$$

Diagrams $d2$, $d3$ and $d4$ are genuine new channels and correspond, respectively, to the processes: $K \rightarrow K ph ph$, $K \rightarrow K ph \Delta h$ and $K \rightarrow K \Delta h \Delta h$. Those processes have the following thresholds: $T_K \geq 222$ MeV $> m_{\pi}$ for diagram $d1$, $T_K > 0$ for diagram $d2$, $T_K \geq 181$ MeV $> m_{\pi}$ for diagram $d3$ and $T_K \geq 392$ MeV $> 2m_{\pi}$ for diagram $d4$.

We do not evaluate the contribution of diagram $d4$ because its threshold is close to the highest energies we consider and we expect it to be small. We have done

the calculations up to second order in density for the processes $K \rightarrow K ph ph$. Higher orders have been considered for $K \rightarrow K \pi ph$, $K \rightarrow K \pi \Delta h$ and $K \rightarrow K ph \Delta h$. But despite that, we have found that their behavior is quadratic in density, so higher order corrections are negligible. In fig. 10, results for $\text{Im}\Pi^{\text{d}1}$ and $\text{Im}\Pi^{\text{d}3}$ with $T_K = 450$ MeV are depicted with crosses for different densities, the lines shown for comparison are exact quadratic functions.

On the other hand in $\text{Im}\Pi^{\text{d}1}$ so far we have considered only the second order terms coming from the iterated ph or Δh excitations like in fig. 2d. Now it is easy to include the diagrams of the same order in the density corresponding to a simultaneous excitation of two particles-two holes by the pion (related to the second order pion proper selfenergy), this contribution is given by diagram $d5$, shown in fig. 11. Its contribution to the imaginary part of the K^+ -selfenergy is given by the same expression than $\text{Im}\Pi^{\text{d}1}$ of eq. (27) where instead of $\text{Im}\delta D$ we are considering $\text{Im}\delta D^{\text{d}5}$, which is the modification of the pion propagator due to the $2p2h$ channel of pion absorption:

$$\begin{aligned}\text{Im}\Pi^{\text{d}5}(k) &= -6 \int \frac{d^3 q}{(2\pi)^3} \int_0^\infty \frac{dq^0}{2\pi} \text{Im}\tilde{t}(u) \text{Im}\delta D^{\text{d}5}(q) , \\ \text{Im}\delta D^{\text{d}5}(q) &= D_0^2(q) \text{Im}\Pi_\pi^{2p2h}(q) ,\end{aligned}\quad (31)$$

where $\text{Im}\Pi_\pi^{2p2h}$ is the pion selfenergy due to the $2p2h$ channel of pion absorption. For this we take the model of [16], which in lowest order in density contains the same input as here, but we have simplified it and rewritten the second order part of it as in ref. [22] which gives rise to about the same results for pionic atoms. Since this selfenergy is for pions on-shell, we modify it by multiplying by the ratio of phase space for $2p2h$ excitation for the off-shell and on-shell situations and by the pion-nucleon squared form-factor $F^2(q)$ (given in appendix A)

$$\begin{aligned}\text{Im}\Pi_\pi^{2p2h}(q) &= -4\pi\mathbf{q}^2 \text{Im}C_0 \rho^2 F^2(q) \frac{\text{phase}(q^0, \mathbf{q})}{\text{phase}(m_\pi, \mathbf{0})} , \\ \frac{\text{phase}(q^0, \mathbf{q})}{\text{phase}(m_\pi, \mathbf{0})} &= \theta(4Mq^0 - \mathbf{q}^2) \sqrt{\frac{4Mq^0 - \mathbf{q}^2}{4Mm_\pi}} + \mathcal{O}(k_F) , \\ \text{Im}C_0 &= 0.096m_\pi^{-6} ,\end{aligned}\quad (32)$$

where the phase-space ratio has been taken at $\rho = 0$. Only the p -wave part of the pionic optical potential has been written, since the s -wave part contribution is much smaller than this for the relevant values of \mathbf{q} involved.

One could also think about effects from the renormalization of the intermediate kaon propagator. The impulse approximation $t_{KN} \rho$ from Appendix C provides the dominant part of the kaon selfenergy. From fig. 5 one can see that $-\text{Im}\Pi(k)/m_K^2 \sim 0.04$ is much smaller than $-\text{Im}\Pi_\pi(k)/m_\pi^2$ and thus the corrections from this source can be estimated reasonably smaller than those obtained from pion renormalization.

The contributions of all MEC diagrams to the imaginary part of the K^+ selfenergy are approximately quadratic in density. In fig. 12 the contribution of each of

the diagrams $d1$, $d2$, $d3$ and $d5$ at density ρ_0 are shown for different kinetic energies of the kaon. Also the total of the MEC contributions, $d1 + d2 + d3 + d5$, is shown. For comparison the exact result for the “standard” calculation, $\text{Im}\delta\Pi = \text{Im}\Pi^{d1}$, is depicted with dashed line. By itself it is much smaller than the total MEC contributions coming from diagrams $d1$, $d2$, $d3$ plus $d5$. The diagram $d2$ is the most important MEC correction for low energies, but for higher energies the most relevant is $d3$, being more than half the total MEC effect for $T_K = 450$ MeV. The contribution of diagram $d5$ is negligible as seen in figure, if we had considered the $\text{Im}C_0$ parameter of the pionic atoms optical potential of eq. (32) to be up to four times larger, such as it is in certain parametrizations found in the literature, its contribution would still be negligible as compare to the total MEC result. In fig. 5 we display the total MEC value together with the value of the IA. We see that the contribution due to the pionic cloud is sizable in relation to the dominant term which comes from the IA. We have checked that these curves are fairly stable under a reasonable modification of the LLEE parameter g' .

The selfenergy $\Pi^{\text{MEC}}(\mathbf{r})$ in finite nuclei is obtained by substituting ρ by $\rho(\mathbf{r})$ in the nuclear matter results. This is shown in ref. [16] to be practical and accurate for the s -wave part, which gives practically the whole contribution here.

The results shown in this section and in section 6 complement and correct our preliminary results exposed in ref. [23]

We have observed that the resonant part of the $t_{K\pi}$ -matrix does not contribute significantly to the imaginary part of the kaon-nucleus optical potential. Its contribution is smaller than one per cent for $T_K \leq 550$ MeV/c. In other words $\text{Im}\Pi^{\text{MEC}}$ is, in very good approximation, proportional to the parameter β'_0 . This parameter is given in the work of [12] by

$$\beta'_0 = -\frac{8\pi}{3}(m_\pi + m_K)(a_1^2 + 2a_3^2),$$

where a_{2I} is the scattering length in the isospin I channel.

Then we can consider a simplified model, which consists of taking a purely constant value for $|t_{K\pi}|^2$, with β'_0 given by the scattering lengths. In particular the quantity $f(u)$ (eq. (58)), relevant for $\text{Im}\Pi^{\text{MEC}}$, is now a constant. In the model of ref. [12] β'_0 is constrained by on-shell data at threshold which are taken from the analysis of ref. [25]. This simplified model saves a lot of computing time because certain integrals in eq. (30) can be done trivially due to the constancy of $f(u)$.

5.- Real part of the K^+ optical potential

Now, let us pay attention to the calculation of the real part of the K^+ selfenergy due to the pionic cloud in the nucleus.

We go back to eq. (12) for $\delta\Pi(k)$ and substitute the isoscalar averaged t -matrix of eq. (15) with its dispersion relation of eq. (16). Then, we consider separately the contributions to $\delta\Pi$ coming from the analytical part of \tilde{t} (this is P) and from

its dispersive part (related to $\text{Im}\tilde{t}$):

$$\delta\Pi = 3i \int \frac{d^4q}{(2\pi)^4} \delta D(q) \left(P(s) + \int_{x_0}^{\infty} \frac{dx}{\pi} \frac{\text{Im}\tilde{t}(x)}{x_0 - x} \frac{s - x_0}{s - x + i\epsilon} \right), \quad (33)$$

where use has been made of crossing symmetry to cancel the factor $1/2$. As $P(s)$ is a real polynomial in q^0 and, by doing a Wick rotation for q^0 as depicted in fig. 4, it can be proved that the first part (that going with $P(s)$) is real. By doing the same Wick rotation, one can see that the second part (going with $\text{Im}\tilde{t}(x)$) is complex, its imaginary part being given by eq. (19). This second part is linear in $\text{Im}\tilde{t}(x)$. Due to the optical theorem $\text{Im}\tilde{t}(x) \propto |\tilde{t}(x)|^2$. So, the first part is of order \tilde{t} and the second one is of order \tilde{t}^2 . We are keeping the leading order contribution to both, $\text{Re}\delta\Pi$ and $\text{Im}\delta\Pi$, this is: order \tilde{t} for $\text{Re}\delta\Pi$ and order \tilde{t}^2 for $\text{Im}\delta\Pi$. Within the same approximation, one should neglect for the real part the contribution of the diagrams $d2$, $d3$ and $d5$. Note that to order $|\tilde{t}|^2$ there would be more diagrams besides these, which do not contribute, or contribute little, to the imaginary part, for instance $d4$.

With this approach of keeping the dominant order in \tilde{t} and considering the incoming K^+ on-shell:

$$\text{Re}\delta\Pi(k) = -3 \int \frac{d^4q}{(2\pi)^4} \text{Im}\delta D(q) P(s) \quad (34)$$

$$= -3 \int \frac{d^3\mathbf{q}}{(2\pi)^3} \int_0^{\infty} \frac{dq^0}{\pi} \text{Im}\delta D(q) \left[\frac{\alpha_0}{2} + \beta_0(m_K^2 + q^{02} - \mathbf{q}^2) \right]. \quad (35)$$

Where we have used

$$P(x) = \frac{\alpha_0}{2} + \beta_0 x, \quad (36)$$

which, in the model of [12], is the dominant contribution to $P(x)$ and comes from the s -wave, the p -wave contribution has been neglected. α_0 , β_0 are given in table 1. In this approximation $\text{Re}\delta\Pi$ is independent of the K^+ kinetic energy. Eq. (35) is the estimation we are going to use for the real part of the K^+ -selfenergy. Observe that for $\text{Re}\delta\Pi$ we have the pion four-momentum without any phase-space restriction. But also notice that the relevant results are coming from the q -values such that $\text{Im}\delta D(q)$ is large, and this happens for small values of \mathbf{q} and q^0 , because in the limit of q large ($\mathbf{q} \rightarrow \infty$ or $q^0 \rightarrow \infty$) the pion selfenergy, which makes $D(q)$ different to $D_0(q)$, goes to zero. For the purpose of evaluating $\text{Re}\delta\Pi$, we split it in different parts as follows:

$$\begin{aligned} \text{Re}\delta\Pi = & \alpha_0 \gamma_1 + 2\beta_0 (\gamma_2 + \gamma_3), \\ \gamma_1 = & -\frac{3}{2} \int \frac{d^3\mathbf{q}}{(2\pi)^3} \int_0^{\infty} \frac{dq^0}{\pi} \text{Im}\delta D(q) \equiv \int \frac{d^3\mathbf{q}}{(2\pi)^3} \frac{\delta N(\mathbf{q})}{2\omega(\mathbf{q})}, \\ \gamma_2 = & -\frac{3}{2} \int \frac{d^3\mathbf{q}}{(2\pi)^3} \int_0^{\infty} \frac{dq^0}{\pi} \text{Im}\delta D(q) (m_K^2 - \mathbf{q}^2) \equiv \int \frac{d^3\mathbf{q}}{(2\pi)^3} \frac{\delta N(\mathbf{q})}{2\omega(\mathbf{q})} (m_K^2 - \mathbf{q}^2), \\ \gamma_3 = & -\frac{3}{2} \int \frac{d^3\mathbf{q}}{(2\pi)^3} \int_0^{\infty} \frac{dq^0}{\pi} \text{Im}\delta D(q) q^{02} \quad . \end{aligned} \quad (37)$$

By doing the numerical evaluation using the pion selfenergy of Appendix A, the results are: $\gamma_1 = 0.02 \text{ fm}^{-2}$, $\gamma_2 = -0.04 \text{ fm}^{-4}$, $\gamma_3 = -0.006 \text{ fm}^{-4}$ evaluated at $\rho = \rho_0$. Notice that $\text{Re}\delta\Pi$ is independent of the energy of the K^+ , then

$$\text{Re}\delta\Pi(k; \mathbf{r}) = \text{Re}\delta\Pi(\mathbf{r}) = \text{Re}\delta\Pi(\rho = \rho_0) \left(\frac{\rho(\mathbf{r})}{\rho_0} \right)^2 \equiv \text{Re}B \left(\frac{\rho(\mathbf{r})}{\rho_0} \right)^2. \quad (38)$$

For the parametrizations I and III of ref. [12], we obtain the values of $\text{Re}\delta\Pi(\rho = \rho_0) \equiv \text{Re}B$ shown in table 1 and fig. 13. $\text{Re}\delta\Pi_{\text{stat}}$ has been obtained by taking the static approximation $q^0 = 0$ in eq. (35), which amounts to taking $\gamma_3 = 0$ in eq. (37). Noting that $\gamma_3/\gamma_2 \simeq 0.15$, we see that this static approximation is not bad in this case. We see that different off-shell extrapolations provide very different results for the real part of the MEC selfenergy of kaons, being possible to obtain different signs for it. $\text{Re}\delta\Pi > 0$ for parametrization I, and $\text{Re}\delta\Pi < 0$ for parametrization III. Parametrization IV is obtained by imposing $\text{Re}\delta\Pi = 0$, which gives $\alpha_0 = -2.8$, $\beta_0 = -0.61 \text{ fm}^2$. Note that α_0 , β_0 are related in order to reproduce the scattering lengths, see Appendix B.

In fig. 13 the real parts calculated at order \tilde{t} are displayed with labels I, III and IV, depending on the parametrization used. The result I is of the same order of the impulse approximation IA, but III is smaller and has different sign. We also present the result of doing the calculation in the spirit of ref. [12], that is, in the static approximation and keeping the whole $\text{Re}\tilde{t}$ (including $P(x)$ and the part related to $\text{Im}\tilde{t}$), in this case we use parametrization I, the result is labeled I_{JK} . We see that I_{JK} is quite different from I, this means than the term coming from $\text{Im}\tilde{t}$ is not small, but we should not calculate one of those contributions but all of them which are of the same order in \tilde{t} .

Given the large sensitivity of the real part to the uncertainties of the off-shell extrapolation for the \tilde{t} -matrix, we think that the computation of the real part is presently beyond the scope of the microscopical approach.

6.- Results: K^+ -nucleus cross section

In fig. 14 we show the results for $\frac{d\sigma}{d\Omega}$ for K^+ with energy $T_K = 450 \text{ MeV}$ scattered by ^{12}C . The result with the impulse approximation is compared to those including pion cloud effects, using parametrizations I and III, the result using parametrization IV, not shown, ($\text{Re}(\Pi^{\text{MEC}}) = 0$) is in between. We find that the inclusion of MEC effects provides some improvement in comparison with the experimental data. In fig. 15 the same is compared for the ^{40}Ca nucleus. The effect of pion cloud is very similar to the case of ^{12}C . In both cases the Coulomb interaction is neglected. Here we show the results in order to see the size and shape of the MEC effects in the differential cross-section. Some other theoretical corrections, as discussed later, should also be included for a proper comparison with experiments.

The total cross-section of K^+ scattered by ^{12}C versus kinetical energy of the K^+ is shown in fig. 16a. The experimental data with a cross are from ref. [8], the

data with a diamond are from ref. [4], only the statistical errors are included, the systematic errors, not shown, are larger. The dashed line labeled IA corresponds to the impulse approximation. The dotted and solid lines include MEC effects using parametrizations I, III and IV. Note that $\text{Im}\Pi^{\text{MEC}}$, as computed in section 3 does not depend on the parametrization.

For low energies the resulting cross-section including MEC depends a lot on the real part of the optical potential and hence on the parametrization used. But it is less dependent for higher energies. Given that the real part is not at all under control from the model, we take hereafter as a reference the line labeled IV, which amounts to neglecting the MEC effects for the real part of the optical potential. Figure 16a shows that the inclusion of MEC effects in the imaginary part significantly improves on the impulse approximation, bringing the cross-section closer to the experimental one, and showing that MEC effects are large enough to have to be considered in this process.

We have used Arndt's phase-shifts [27]. The calculated K^+ nucleus total cross section would have been larger if we had used Martin's [26] phase shifts rather than Arndt's [27] for the KN scattering amplitudes as shown in ref. [2]. The analysis of [27] is more recent than the one in [26]. On the other hand a recent reanalysis [28] of the KN data seems to favor Martin's phase shifts.

These theoretical uncertainties in the K^+ -nucleus cross-sections partially cancel if a quotient of cross-sections is taken. Same is true for systematic errors in the experimental measurements of the total K^+ -nucleus cross-sections. Then, the magnitude usually calculated and compared with the experiment in most of research works is the ratio over the K^+ deuterium total cross-section: $R[A] = \frac{\sigma(K^+ A)}{(A/2)\sigma(K^+ {}^2H)}$ for a nucleus of mass number A . In particular for ${}^{12}C$ the following ratio R is defined:

$$R = \frac{\sigma(K^+ {}^{12}C)}{6\sigma(K^+ {}^2H)}, \quad (39)$$

where the factor 6 in the denominator is included to emphasize the closeness of the ratio to unity.

One should notice that for the magnitude R , being a quotient of cross-sections, the possible uncertainties due to the use of different phase-shifts partially cancel and they are not relevant. So we present in fig. 16b the same results as in fig. 16a but for the ratio R , which has less error than the total cross section. The dashed line correspond to the IA calculation, and the other lines include IA+MEC, using for MEC effects the parametrizations I, III and IV as labeled.

So far we have calculated MEC effects on the total K^+ -nucleus cross-section for ${}^{12}C$. We have shown that these effects are large enough as compared to the IA approximation and, then, they need to be considered.

But, for doing a meaningful comparison of theoretical calculations with experiments, a more realistic K^+ -nucleus standard optical potential (than the crude $t\rho$ impulse approximation used in fig. 14-16) should be considered. There are corrections over this $t\rho$ which should be included like off-shell range, binding energy,...

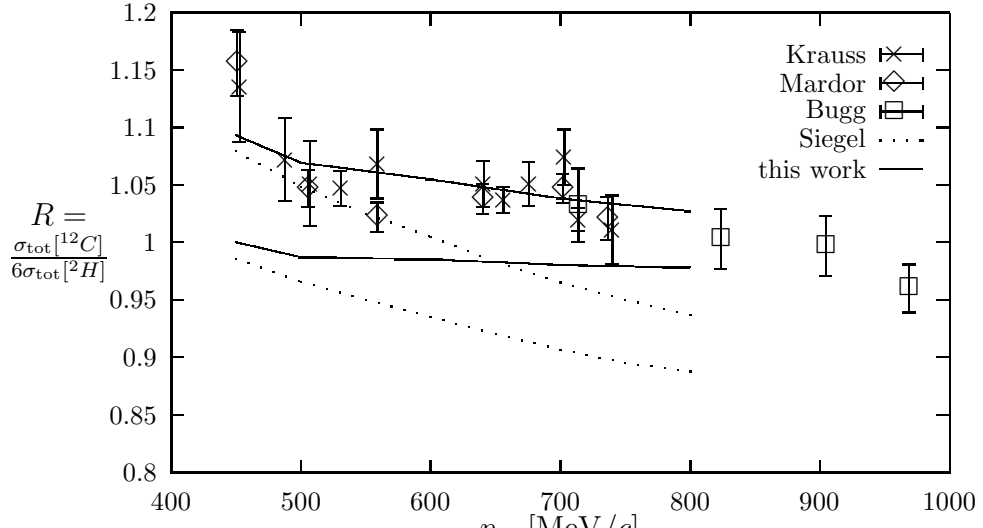


figure 17

Also, there are nucleon-nucleon correlations which contribute to the optical potential in second order. These correlation effects are approximately ρ^2 by nature, which is the same form as the MEC contributions to the optical potential.

Both kinds of corrections to the optical potential (and their effect on the K^+ -nucleus cross-sections) have been calculated and/or estimated in the works of Siegel, Kaufmann and Gibbs [1, 2]. As result of their studies, they provide a band of uncertainty for the conventional calculation, the boundaries of the band are determined by varying the parameters in the theoretical model.

We show in fig. 17 with dashed-lines the band of theoretical calculations for R with the conventional microscopic optical potential of ref. [2], for $p < 500$ MeV/c the results quoted are from ref. [6]. The solid lines band in fig. 17 shows the effect of adding our MEC correction to the multiple scattering calculation of ref. [2]. This correction is obtained by taking:

$$\Delta R^{\text{MEC}} = \frac{\Delta\sigma^{\text{MEC}}(^{12}C)}{6\sigma(^2H)}, \quad (40)$$

where $\Delta\sigma^{\text{MEC}}(^{12}C) = \sigma^{\text{IA+MEC}}(^{12}C) - \sigma^{\text{IA}}(^{12}C)$, and $\sigma(^2H)$ has been obtained directly from the Arndt phase-shifts by taking $\sigma(^2H) = \sigma_n + \sigma_p$. In calculating the MEC correction we have taken only its contribution to the imaginary part of the optical potential, while no correction has been done to the real part. We observe that the addition of MEC correction to the conventional optical calculation of Siegel *et al.* provides a significative agreement of the calculation with the experiment for a large range of energies.

7.- Conclusions

Let us summarize the results of our calculation. We have computed the pionic cloud contribution to the K^+ -nucleus selfenergy at lowest order in $t_{K\pi}$ (see sections 4 and 5). Our result is well described for $T_K < 2.5 \text{ fm}^{-1}$ by:

$$\Pi^{\text{MEC}}(T_K, \mathbf{r}) = B(T_K) \left(\frac{\rho(\mathbf{r})}{\rho_0} \right)^2, \quad (41)$$

where the coefficient $B(T_K)$ is complex and T_K is the kinetic energy of the incoming K^+ . We have found that, within our approximation, $\text{Re}B$ is energy independent. Its precise value is not known due to the uncertainties in the off-shell extrapolation of the $K\pi$ amplitudes (see Table 1). On the other hand, with very good approximation, $\text{Im}B(T_K)$ can be cast in the following form:

$$\text{Im}B(T_K) = \beta'_0 \{ k_1 T_K + k_2 (T_K - T_0) \theta(T_K - T_0) \}, \quad (42)$$

with $k_1 = 3.0 \cdot 10^{-3} \text{ fm}^{-2}$, $k_2 = 2.0 \cdot 10^{-2} \text{ fm}^{-2}$, and $T_0 = 1.0 \text{ fm}^{-1}$. The constant k_1 is related to the diagram d_2 , and k_2 to the rest of the calculated MEC diagrams d_1 , d_3 , d_5 which contribute to $\text{Im}B$ above a threshold of around T_0 as stated by the step function $\theta(T_K - T_0)$. β'_0 is related to the $K^+\pi$ scattering lengths. For the model of refs. [12, 25], one obtains $\beta'_0 = -8.1 \text{ fm}$. The K^+ -nucleus data for ^{12}C are well reproduced for all energies by $\text{Re}B=0$, $\beta'_0 = -8.1 \text{ fm}$, as can be seen in fig. 17, when conventional nuclear corrections, taken from ref. [2], are included together with the MEC effects.

The main conclusion of this paper is that the effects of the mesonic cloud in K^+ nucleus scattering are relevant and of the right order of magnitude to account for the discrepancies of the conventional optical potential [2] with the data. However, there are uncertainties, particularly in the real part of the MEC, which do not allow us to draw stronger conclusions about the actual size of the corrections. The main reason is the sensitivity of the results to the off-shell extrapolation of the KN scattering matrix for which there is not yet enough information. Furthermore, we also noted that there are other sources of real part, not linear in the KN t -matrix, which should also be considered. Our evaluation of the imaginary part was however very precise within the model of ref. [12] used here. However, there are also approximations in $\text{Im}t_{K\pi}$ of ref. [12] since the parameter β'_0 is tied to the threshold $K\pi$ amplitudes only. Other models for the amplitude would also provide different results for $\text{Im} \Pi^{\text{MEC}}$ although the restricted phase space for $\text{Im} \Pi^{\text{MEC}}$ and the on-shell constraints in the amplitude make this magnitude more stable.

The comparison of our results using $\text{Re} \Pi^{\text{MEC}} = 0$ with the data is very good.

On the other hand we also have observed that the direct relation of Π^{MEC} to the distribution of excess pions in the nucleus, as has been formerly assumed, is a consequence of a dangerous static approximation which should be avoided. In the present case it induced an error of a factor of two but in other cases it can induce errors of several orders of magnitude. We also found that in any case this contribution was only a small part of the total MEC corrections tied to the interaction of kaons with the nuclear pions. These findings should also serve as

a warning for other calculations directly relating the pion excess number to the modification of nuclear magnitudes from the interaction of particles with the meson cloud.

Acknowledgements:

We thank to L.L. Salcedo, D.D. Strottman, M.J. Vicente-Vacas, W. Weise and A. Steiner for helpful discussions and suggestions. Partial financial support has been obtained from the following sources: DGICYT (Spain) research project number PB92-0927 of the University of Granada, CICYT (Spain) research project AEN93-1205 of the University of Valencia, Junta de Andalucia and INT University of Washington.

Appendix A.- The pion propagator

We have taken

$$D(q) = [q^0 - \mathbf{q}^2 - m_\pi^2 - \Pi_\pi(q^0, \mathbf{q})]^{-1}, \quad (43)$$

where

$$\begin{aligned} \Pi_\pi(q) &= \mathbf{q}^2 \frac{\alpha(q)}{1 - g'\alpha(q)}, \\ \alpha(q) &= \alpha_N(q) + \alpha_\Delta(q), \\ \alpha_N(q) &= \left(\frac{f(q)}{m_\pi}\right)^2 U_N(q), \\ \alpha_\Delta(q) &= \left(\frac{f(q)}{m_\pi}\right)^2 U_\Delta(q), \\ f(q) &= f_\pi F(q) = f_\pi \frac{\Lambda^2}{\Lambda^2 + \mathbf{q}^2}, \end{aligned} \quad (44)$$

where $1 - g'\alpha(q)$ is the Lorentz-Lorenz factor, with g' the Landau-Migdal parameter, and U_N, U_Δ , the Lindhard functions for ph and Δh excitation with the appropriate normalization are given explicitly in the appendix of [29]. $U_\Delta(q)$ has an imaginary part coming from Δ decay into πN . We have taken the form factor static because the relevant momenta involved in the process are well below Λ and the form factor does not play much of a role. This was already investigated in [12]. Not having q^0 dependence in $F(q)$ simplifies the analytical structure and allows us to make the formal developments of the former sections. We take $g' = 0.6$, $f_\pi^2/4\pi = 0.08$, and $\Lambda = 1250$ MeV.

The leading order in density of $\Pi_\pi^{(1)}$ is given by:

$$\Pi_\pi^{(1)} = \Pi_N + \Pi_\Delta, \quad \Pi_N(q) = \mathbf{q}^2 \alpha_N^{(1)}, \quad \Pi_\Delta(q) = \mathbf{q}^2 \alpha_\Delta^{(1)},$$

where $\alpha_N^{(1)}$ and $\alpha_\Delta^{(1)}$ are the linear part in density of α_N and α_Δ of eq. (44). Hence, the leading orders in density expansion for the pion propagator $D(q)$ are:

$$\begin{aligned} D_{(1)}(q) &= D_0^2(q) \Pi_\pi^{(1)} = D_{(1)}^{ph} + D_{(1)}^{\Delta h}, \\ D_{(1)}^{ph}(q) &= D_0^2(q) \Pi_N(q), \quad D_{(1)}^{\Delta h}(q) = D_0^2(q) \Pi_\Delta(q), \\ D_{(2)}(q) &= D_0^2(q) \mathbf{q}^2 \alpha^2(q) (g' + \mathbf{q}^2 D_0(q)), \end{aligned}$$

Appendix B.- The $K^+\pi$ amplitude.

As discussed before we need only the isoscalar $K\pi$ amplitude which we take from [12]. This amplitude incorporates analytical properties, unitarity, crossing symmetry $t^0(k', q'; k, q) = t^0(k', -q; k, -q')$, and on-shell constraints and keeps up to linear terms in s and u for forward scattering. Its justification and uncertainties are clearly discussed in [12] and we refer the reader to this paper. The model

contains an s -wave part and a p -wave part. The p -wave part is accounted for by means of a $l = 1/2$ resonance, $K^*(892)$. After the implementation of the crossing symmetry the two pieces give rise to the following isoscalar amplitude.

$$t^0(k, q; k, q) = t^{(0,s)}(k, q; k, q) + t^{(0,p)}(k, q; k, q), \quad (45)$$

$$t^{(0,s)}(k, q; k, q) = \alpha_0 + \beta_0(s + u) + i\beta'_0[k(s) + k(u)], \quad (46)$$

$$t^{(0,p)}(k, q; k, q) = T_{\text{res}}(s)\theta(s - x_0) + T_{\text{res}}(u)\theta(u - x_0), \quad (47)$$

with

$$T_{\text{res}}(x) = -\frac{8\pi\sqrt{x}}{K(x)} \frac{M_r\Gamma(K(x))}{M_r^2 - x - iM_r\Gamma(K(x))}, \quad (48)$$

$$\Gamma(K) = \left(\frac{K}{K_r}\right)^3 \Gamma_r \left[\frac{1 + (K_r R)^2}{1 + (KR)^2} \right], \quad (49)$$

$x_0 = (m_K + m_\pi)^2$ and $k(x)$, $K(x)$ the CM momentum given by

$$k(x) = \frac{\sqrt{m_\pi m_K}}{m_\pi + m_K} \sqrt{x - (m_\pi + m_K)^2}, \quad (50)$$

$$K(x) = \left[\frac{[x - (m_\pi + m_K)^2][x - (m_\pi - m_K)^2]}{4x} \right]^{1/2} \quad (51)$$

and the parameters: $\beta'_0 = -8.1$ fm, $M_r = 895.7$ MeV, $\Gamma_r = 52.9$ MeV, $R = 4.3$ $(\text{GeV}/c)^{-1}$, K_r given by eq. (51) for $x = M_r$. Three different parametrizations I, II and III, with values for α_0 , β_0 , given in table 1 are taken from [12]. These parameters are constrained by the relationship $\alpha_0 + 2(m_\pi^2 + m_K^2)\beta_0 = -11.0$, which follows from eq. (46) on-shell and at threshold. Notice that parametrization II does not fulfill this requirement. So we will not use it.

Note that $K(x)$ is the relativistic CM momentum while $k(x)$ involves a non-relativistic approximation. The choice of $k(x)$ for the s -wave part is done in [12] to avoid extra singularities and is consistent with some threshold approximations involved in the derivation of eq. (46).

Since $T_{\text{res}}(x)$ is zero below pion threshold there are no problems in separating the real and imaginary parts. However, the imaginary part in the s -wave term gives rise to a real part below pion threshold when extrapolated analytically. Thus

$$t^{(0,s)}(k, q; k, q) = \tilde{t}^{(0,s)}(s) + \tilde{t}^{(0,s)}(u) \quad (52)$$

with

$$\begin{aligned} \text{Re } \tilde{t}^{(0,s)}(x) &= \begin{cases} \frac{\alpha_0}{2} + \beta_0 x & , x > x_0 \\ \frac{\alpha_0}{2} + \beta_0 x - \beta'_0 k_I(x) & , x < x_0 \end{cases} \\ \text{Im } \tilde{t}^{(0,s)}(x) &= \begin{cases} \beta'_0 k(x) & , x > x_0 \\ 0 & , x < x_0 \end{cases} \end{aligned} \quad (53)$$

with

$$k_I(x) = \frac{\sqrt{m_\pi m_K}}{m_\pi + m_K} \sqrt{x_0 - x}. \quad (54)$$

Coming back to eqs. (28) and (29), we discussed that in the general case for $u > (m_\pi + m_K)^2$.

$$\sum_l \sum_{i,j} |t_{K^+ \pi^l \rightarrow K^i \pi^j}(k', q'; k, -q)|_{\text{ave}}^2 = -\frac{8\pi\sqrt{u}}{K(u)} 3 \text{Im } \tilde{t}(u) \quad (55)$$

$$= -24\pi \left\{ \sqrt{u} \frac{k(u)}{K(u)} \beta'_0 - \text{Im} \frac{8\pi u}{K^2(u)} \frac{M_r \Gamma(K(u)) \theta(u - x_0)}{M_r^2 - u - iM_r \Gamma(K(u))} \right\}, \quad (56)$$

with $u = (k - q)^2$. However, the threshold approximations involved in the s-wave part in [12] require that all factors in the s-wave part in eq. (56) be calculated at pion threshold. We have checked that this induces about 5% differences in the evaluation of the diagram of fig. 2a with respect to the results keeping the u dependent factors. Observe that eq. (56) provides the analytical continuation of the left hand side of eq. (55) for $u < (m_\pi + m_K)^2$.

Note that if the factor \sqrt{u} is kept we run into problems if the line q' excites a ph , like in diagrams $d1, d2, d3$ of fig. 9, since u can become negative and this leads to the absurd conclusion that $|t^2|$ is purely imaginary. The threshold approximations done in [12] aimed at avoiding such pathologies.

Thus, taking this into account this average we can rewrite eq. (23) in the form:

$$\begin{aligned} \text{Im} \tilde{\Pi}(k) &= 2 \int \frac{d^4 q}{(2\pi)^4} \int \frac{d^4 q'}{(2\pi)^4} \theta(q^0) \theta(q'^0) \theta(k^0 - q^0 - q'^0) \\ &\times f(u) \text{Im} D(q) \text{Im} D(q') \text{Im} D_K(k - q - q'), \end{aligned} \quad (57)$$

$$f(u) = -24\pi \left\{ \beta'_0(m_\pi + m_K) - \frac{8\pi u}{K^2(u)} \text{Im} \frac{M_r \Gamma(K(u)) \theta(u - x_0)}{M_r^2 - u - iM_r \Gamma(K(u))} \right\}. \quad (58)$$

For the s -wave this is equivalent to consider the on-shell values for the $t_{K\pi}$ -matrix when calculating $|t|^2$ but evaluated at threshold.

Appendix C.- The impulse approximation

Our K^+ selfenergy in the impulse approximation is given by

$$\Pi^{(\text{IA})}(k) = -\frac{4\pi\sqrt{s}}{M} \left\{ \frac{1}{2} (f_0 + f_1) \rho_n(\mathbf{r}) + f_1 \rho_p(\mathbf{r}) \right\}, \quad (59)$$

with M the nucleon mass, where f_I are the $K^+ N$ spin non flip isospin amplitudes and $\rho_n(\mathbf{r}), \rho_p(\mathbf{r})$ the neutron and proton densities.

We consider s, p and d waves. For the p -wave we substitute

$$\mathbf{q} \cdot \mathbf{q}' \rho(\mathbf{r}) \rightarrow -\frac{M^2}{s} \nabla \rho(\mathbf{r}) \nabla, \quad (60)$$

as customarily done in pionic atoms [30], and for the d -wave, which is almost negligible in the range that we study, we take only the forward value in eq. (59).

The $K^+ N$ phase shifts are taken from [27]. The kaon selfenergy in the impulse approximation is shown in figs. 5 and 13 for nuclear matter density.

Table 1

	α_0 [fm 2]	β_0 [fm]	β'_0 [fm]	$\text{Re}\delta\Pi_{\text{stat}}(\rho = \rho_0)$ [fm $^{-2}$]	$\text{Re}\delta\Pi(\rho = \rho_0)$ $\equiv \text{Re}B$ [fm $^{-2}$]
I	18.7	-2.2	-8.1	0.54	0.58
II	11.4	-1.0	-8.1		
III	-11.0	0.0	-8.1	-0.22	-0.22
IV	-2.8	-0.6	-8.1	\sim 0.00	0.00

- **Table 1:** Different parametrizations for the $K - \pi$ t -matrix, and the results of the real part of the K^+ optical potential due to the pionic cloud for normal nuclear matter for each parametrization.

Figures captions

- **Figure 1:** $\delta N(\mathbf{q})$ versus q is shown for normal nuclear matter.
- **Figure 2:** “Standard” K^+ selfenergy diagrams due to the pion cloud.
- **Figure 3:** K^+ scattering with a pion, annihilating two pions from the ground state or creating two pions from the ground state.
- **Figure 4:** The complex plane q^0 with the cuts and poles of $D(q)\tilde{t}(u)$. The adequate Wick rotation for performing its integration in q^0 is shown.
- **Figure 5:** Imaginary part of the K^+ selfenergy for normal nuclear matter versus kinetic energy of the incoming kaon.
- **Figure 6:** The optical theorem for the $K\pi$ amplitude is diagrammatically shown.
- **Figure 7:** Feynman diagram which imaginary part is related, through the optical theorem, to the imaginary part of the “standard” diagram of fig. 2.
- **Figure 8:** This diagram contains all the contributions to the imaginary part of the K^+ selfenergy up to second order in $t_{K\pi}$.
- **Figure 9:** Diagrams $d1$, $d2$, $d3$ and $d4$. They contribute to $\text{Im}\Pi^{\text{MEC}}$ up to second order in density.
- **Figure 10:** Imaginary part of the K^+ selfenergy versus density for 450 MeV of kinetic energy of the incoming kaon for diagrams $d1$ and $d3$ are shown. The lines are exact quadratic functions in density for comparison.
- **Figure 11:** Diagram $d5$. It contributes to $\text{Im}\Pi^{\text{MEC}}$ in second order in density.
- **Figure 12:** Imaginary part of the K^+ selfenergy for normal nuclear matter versus kinetic energy of the incoming kaon from the different mechanisms considered.
- **Figure 13:** Real part of the K^+ selfenergy for normal nuclear matter versus kinetic energy of the incoming kaon.
- **Figure 14:** Differential cross section of a K^+ with kinetic energy of 450 MeV scattered by a ^{12}C nucleus. Dashed line depicts the results using the IA. Long-dashed (dot-dashed) line includes IA plus the the optical potential coming from the pionic cloud using parametrization I (III). The experimental data are from ref. [5].
- **Figure 15:** Same as fig. 14 for ^{40}Ca . The experimental data are from ref. [6].

- **Figure 16:** a) Total cross section for K^+ scattered by ^{12}C versus kinetic energy of the K^+ . b) The ratio $R = \frac{\sigma(K^+ \text{ } ^{12}\text{C})}{6\sigma(K^+ \text{ } ^2\text{H})}$ versus the lab momentum of the K^+ . Dashed line corresponds to IA. Solid line (IV) includes IA plus the imaginary part of the optical potential coming from the pionic cloud. Dotted lines includes IA plus the imaginary and real parts of the optical potential coming from the pionic cloud for two different parametrizations (I, III) of the $t_{K\pi}$ amplitude. The experimental data are: crosses from ref. [8], diamonds from ref. [4], squares from ref. [6].
- **Figure 17:** The ratio of cross-sections $R = \frac{\sigma(K^+ \text{ } ^{12}\text{C})}{6\sigma(K^+ \text{ } ^2\text{H})}$ is plotted against the lab momentum of the incoming K^+ . The experimental data are: crosses from ref. [8], diamonds from ref. [4], squares from ref. [6]. The two dashed lines define the band of uncertainties of the theoretical results for R obtained with the conventional optical potential of ref. [2]. The two solid lines define the band of uncertainties of the theoretical results for R when the corrections due to MEC calculated here are added to the results obtained with the conventional optical potential of ref. [2].

paper has 17 FIGURES, only fig.17 is included in this LaTeX file
 please, REQUEST THE FIGURES to C. Garcia-Recio, e-mail: G_RECIO@UGR.ES

References

- [1] P. B. Siegel, W. B. Kaufmann and W. R. Gibbs, Phys. Rev. C **30**, 1256 (1984).
- [2] P. B. Siegel, W. B. Kaufmann and W. R. Gibbs, Phys. Rev. C **31**, 2184 (1985).
- [3] C. M. Chen and D. J. Ernst, Phys. Rev. C **45**, 2019 (1992).
- [4] D. V. Bugg et al., Phys. Rev. **168**, 1466 (1968).
- [5] D. Marlow et al., Phys. Rev. C **25**, 2619 (1982).
- [6] Y. Mardor et al., Phys. Rev. Lett. **65**, 2110 (1990).
- [7] J. Alster, Proc. if the Int. Conference on Hypernuclear and Strange Particle physics, Shimoda, Japan, 1991 [Nucl. Phys. **A547**, 321c (1992)].
- [8] R. A. Krauss et al., Phys. Rev. C **46**, 2019 (1992).
- [9] G. E. Brown, C. B. Dover, P. B. Siegel and W. Weise, Phys. Rev. Lett. **60**, 2723 (1988).
- [10] W. Weise, Nuovo Cimento **102A**, 265 (1989).
- [11] S. V. Akulinichev, Phys. Rev. Lett. **68**, 290 (1992).
- [12] M. F. Jiang and D. S. Koltun, Phys. Rev. C **46**, 2462 (1992).
- [13] B. R. Martin, D. Morgan and G. Shaw, Pion- Pion Interaction in Particle Physics (Academic Press, New York, 1976) chap 14.1 and 14.3.
- [14] E. L. Berger, F. Coester and R. B. Wiringa, Phys. Rev. D **29**, 398 (1984); E. L. Berger and F. Coester, Phys. Rev. D **32**, 1071 (1985).
- [15] B. L. Friman, V. R. Pandharipande and R. B. Wiringa, Phys. Rev. Lett **51**, 763 (1983).
- [16] J. Nieves, E. Oset and C. García-Recio, Nucl. Phys. **A554**, 509 (1993); *ibid* pag. 554.
- [17] C. Itzykson and J. B. Zuber, Quantum Field Theory, McGraw Hill, 1985.
- [18] M. Ericson and M. Rosa-Clot, Phys. Lett. B **188**, 11 (1987).
- [19] A. D. Martin and T. D. Spearman, "Elementary Particle Theory", North-Holland, 1970, Amsterdam.
- [20] P. Fernández de Córdoba and E. Oset, Nucl. Phys. **A554**, 793 (1992).

- [21] H. Bando and H. Takaki, Phys. Lett. B **150** , 409 (1985).
- [22] O. Meirav, E. Friedman, R. R. Johnson, R. Olszewski and P. Weber, Phys. Rev. C **40**, 843 (1989).
- [23] C. García-Recio, J.M. Nieves and E. Oset, Act. Phys. Polonica B **24**, 1757 (1993).
- [24] E. Friedman, Act. Phys. Polonica B **24**, 1673 (1993).
- [25] P. Estabrooks *et al.*, Nucl. Phys. B133, 490 (1978).
- [26] B. Martin, Nucl. Phys. **B94**, 413 (1975).
- [27] R. A. Arndt, L. D. Roper and P. II. Steinberg, Phys. Rev.D **18**, 3278 (1978); R. A. Arndt and L. D. Roper, Phys. Rev. D **31**, 2230 (1985).
- [28] Q. Daffner, Diplomarbeit, University of Regensburg, 1990; W. Weise, Private communication.
- [29] E. Oset, P. Fernández de Córdoba, L. L. Salcedo and R. Brockmann, Phys. Reports **188**, 79 (1990).
- [30] M. Ericson and T.E.O. Ericson, Ann. Phys. (N.Y.) **36**, 323 (1966).

This figure "fig1-1.png" is available in "png" format from:

<http://arxiv.org/ps/nucl-th/9407041v1>

This figure "fig2-1.png" is available in "png" format from:

<http://arxiv.org/ps/nucl-th/9407041v1>

This figure "fig3-1.png" is available in "png" format from:

<http://arxiv.org/ps/nucl-th/9407041v1>

This figure "fig4-1.png" is available in "png" format from:

<http://arxiv.org/ps/nucl-th/9407041v1>

This figure "fig5-1.png" is available in "png" format from:

<http://arxiv.org/ps/nucl-th/9407041v1>

This figure "fig1-2.png" is available in "png" format from:

<http://arxiv.org/ps/nucl-th/9407041v1>

This figure "fig2-2.png" is available in "png" format from:

<http://arxiv.org/ps/nucl-th/9407041v1>

This figure "fig3-2.png" is available in "png" format from:

<http://arxiv.org/ps/nucl-th/9407041v1>

This figure "fig4-2.png" is available in "png" format from:

<http://arxiv.org/ps/nucl-th/9407041v1>

This figure "fig5-2.png" is available in "png" format from:

<http://arxiv.org/ps/nucl-th/9407041v1>

This figure "fig1-3.png" is available in "png" format from:

<http://arxiv.org/ps/nucl-th/9407041v1>

This figure "fig2-3.png" is available in "png" format from:

<http://arxiv.org/ps/nucl-th/9407041v1>

This figure "fig3-3.png" is available in "png" format from:

<http://arxiv.org/ps/nucl-th/9407041v1>

This figure "fig4-3.png" is available in "png" format from:

<http://arxiv.org/ps/nucl-th/9407041v1>

This figure "fig1-4.png" is available in "png" format from:

<http://arxiv.org/ps/nucl-th/9407041v1>

This figure "fig2-4.png" is available in "png" format from:

<http://arxiv.org/ps/nucl-th/9407041v1>

This figure "fig3-4.png" is available in "png" format from:

<http://arxiv.org/ps/nucl-th/9407041v1>

This figure "fig4-4.png" is available in "png" format from:

<http://arxiv.org/ps/nucl-th/9407041v1>